ANNALS OF GEOPHYSICS, 65, 5, PA536, 2022; doi: 10.4401/ag-8821
OPEN ACCESS

WWLLN Data Used to Model the Global Ionospheric Electric Field Generated by Thunderstorms

Valery V. Denisenko[1], Michael J. Rycroft[*,2]

(1) Institute of Computational Modelling RAS SB, Krasnoyarsk 660036, Russia
(2) CAESAR Consultancy, Cambridge CB3 9HW, UK

Article history: received March 14, 2022; accepted July 8, 2022

Abstract

Electric currents flowing in the atmospheric global electric circuit (GEC) are closed by ionospheric currents. The physical and mathematical approach to simulate the ionospheric potential which drives these currents has been described in our previous papers. Only the internal electric fields and currents generated by thunderstorms are studied, and without any magnetospheric current sources or generators. The atmospheric conductivity profiles with altitude are empirically determined, and the topography of the Earth's surface is taken into account. A two-dimensional approximation of the ionospheric conductor is based on the high conductivity along the geomagnetic field; the Pedersen and Hall conductivities are calculated using empirical models. The potentials in the E- and F-layers of the ionosphere are considered to be constant along each magnetic field line.
The main progress in comparison with previous versions of the model is obtained through applying the global distribution of thunderstorms obtained from the ground-based World Wide Lightning Location Network. Under typical conditions for July, under low solar activity in 2008, at 18:00 UTC, the calculated maximum potential difference in the ionosphere is 54 V. This newest version of our model contains the equatorial electrojets. There are day-time electrojets, the strengths of which are up to 65 A, and night-time ones (of up to 40 A), while the total current flowing in the GEC is taken to be equal to 1.43 kA in our model to satisfy the Carnegie curve, i.e. the diurnal variation of the vertical electric field at ground level with UTC. The maximum of the electric potential is shifted from Africa to South-East Asia in the new model. The equatorial electrojets also change their position, direction and intensity.

Keywords: Global Electric Circuit; Ionosphere; Electric Field; Numerical Simulation

1. Introduction

There are several mechanisms by which an ionospheric electric field may be generated. First of all, there are magnetohydrodynamic processes operating in the magnetosphere, associated with the movements of the ionospheric medium [Klimenko and Klimenko, 2012]. There are also ionospheric electric fields due to the currents flowing up from the atmosphere [Hays and Roble, 1979]. The currents produced by all these generators are referred to as the global electric circuit (GEC). Here we study only that part of the GEC which is generated by thunderstorms

and other charge-separating clouds. Although numerous articles analyze the thunderstorm-related part of the GEC, its ionospheric part is still insufficiently studied.

The objective of this paper is to present our model for electric fields and currents which constitute the ionospheric part of the thunderstorm-related part of the GEC. The first results of our modelling efforts were presented in [Denisenko et al., 2019a], with corrections [Denisenko et al., 2019b]. Here we briefly describe the model, and then we present some new results which are obtained using a model for the global distribution of thunderstorms [Denisenko and Lyakhov, 2021] obtained from the ground-based World Wide Lightning Location Network (WWLLN). The main key features of the WWLLN system are presented in [Rodger et al., 2004] and on the website https://wwlln.net.

Lightning flash rates are also observed by the Optical Transient Detector (OTD) on the Microlab-1 satellite launched in 1995 and the Lightning Imaging Sensor (LIS) on board the Tropical Rainfall Measuring Mission (TRMM) satellite, launched in 1997. There are different methods of processing these data in their relation to the GEC [Peterson et al., 2021]. Many papers are devoted to the comparison of WWLLN and OTD/LIS data [Rudlosky and Shea, 2013, Lunxiang et al., 2013] and their applications in GEC simulation [Hutchins et al., 2014]. Their general features, such as the maximum flash rate at 15-19 UT, are similar [Minobe et al., 2020], but details differ. It would be interesting to study both of these data sets in the framework of our model, but here we use only WWLLN data, as an example of modern data, in contrast with an earlier and simpler model [Hays and Roble, 1979] which we used in previous versions of our model.

2. The current continuity equation

For our purposes here we regard the atmosphere, ionosphere and magnetosphere as a single conductor. The basic equations for the steady state electric field **E** and current density **j** are Faraday's law, the charge conservation law, and Ohm's law,

$$curl\, \boldsymbol{E} = 0 \tag{1}$$

$$div\, \boldsymbol{j} = Q \tag{2}$$

$$\boldsymbol{j} = \hat{\boldsymbol{\sigma}}\boldsymbol{E} \tag{3}$$

where $\hat{\boldsymbol{\sigma}}$ is the conductivity tensor whose components are described in Section 4. The given function Q differs from zero if an external electric current density $\boldsymbol{j}_{ext}$ exists. Then the total current density is equal to $\boldsymbol{j} + \boldsymbol{j}_{ext}$ and Eq. (2) with $Q = -div\, \boldsymbol{j}_{ext}$ is the charge conservation law for the total current. One can say that Q is the local time derivative of the electric charge density injected by an external current, which must be compensated by the current associated with the conductivity in a steady state process. Since the vector function $\boldsymbol{E}$ satisfies Eq. (1), the electric potential V can be introduced so that

$$\boldsymbol{E} = -grad\, V. \tag{4}$$

Then the system of the equations Eq. (1-3) is reduced to the current continuity equation

$$-div(\hat{\boldsymbol{\sigma}}\, grad\, V) = Q. \tag{5}$$

We use spherical geomagnetic coordinates θ_m, φ_m, geomagnetic latitude $\lambda_m = \pi/2 - \theta_m$ and height above mean sea level h to specify a point. To identify a magnetic field line we use the parameter H which is the height h of its apex.

3. Separation of Ionospheric and Atmospheric Conductors

The lower boundary of the atmosphere is the Earth's surface; our model of the topography is presented in detail in [Denisenko and Yakubailik, 2015]. The conductivity of surface air is much smaller than the conductivities of the continental surface and sea water. Hence the Earth's surface is usually regarded as an ideal conductor in comparison, which means that it is at a constant electric potential V_0, to be defined later. Since the ionospheric conductivity is many orders of magnitude larger than the atmospheric conductivity [Kudintseva et al., 2016], the ionosphere can be approximated as an ideal conductor with zero potential when it is the atmosphere which is simulated. These boundary conditions complete the Dirichlet boundary value problem for equation (5). The problem has a unique solution when the constant V_0 is given. The solution obtained gives the fair weather electric field near the ground. The value V_0 is taken to balance the total fair weather current and thunderstorm currents between the ground and the ionosphere.

We use the height distributions of the atmospheric fair weather conductivity $\sigma(h)$ presented in [Denisenko et al., 2019a] as an average empirical model. Such a model with a given potential difference between the ground and the ionosphere V_0 defines the global distribution of the fair weather currents. In accordance with the Carnegie curve for the diurnal UTC variation of the electric field above the ground [see Fig. 7, Harrison, 2013], the typical vertical electric field strength in air near the ground is $E_0 = 130$ V/m, if one interpolates for July data in Figs. 7 c,d, or $E_0 = 110$ V/m in Fig. 7 g. We take $E_0 = 130$ V/m in the actual model that corresponds to the voltage from the ground to the ionosphere of $V_0 = 250$ kV for our model of the atmospheric fair weather conductivity. The corresponding vertical current density $j_0 = 2$ pA/m^2. All of these numerical values are consistent with those given by [Rycroft et al., 2000].

In view of the linearity of the model one can multiply all resulting electric fields and currents by any common positive number, e.g., by 0.846 to make $E_0 = 110$ V/m instead of 130 V/m. We use the model [Denisenko and Lyakhov, 2021] of the global distribution of thunderstorm activity obtained from the global network of ground-based very low frequency radio receivers WWLLN. The data are separated and averaged for July 2008 for the interval 17:00-19:00 UTC, centered on 18:00 UTC. Here we have chosen this moment of time for the simulations as being typical and simple for comparison with our previous model, in order to demonstrate the importance of having a detailed model for the distribution of thunderstorm currents. Since it is not possible to make direct global measurements of the current passing into the ionosphere from thunderstorm clouds, it is usually assumed that the current into the ionosphere and the number of lightning flashes are proportional to some hidden parameter that characterizes thunderstorm activity. Thus, we use the global distribution of lightning activity as a proxy for the thunderstorm current as described in [Denisenko and Lyakhov, 2021].

The total resistance of the atmosphere for the conductivity model used is found to be about $R = 179$ Ω and the total current flowing down through the atmosphere is $I = V_0/R = 1.43$ kA. In view of the charge conservation law, thunderstorms are considered to provide a balancing current, flowing up, of $I_{atm} = -I = 1.43$ kA. This value defines the coefficient of proportionality between the lightning flash rate and the current into the ionosphere.

The global distribution of the thunderstorm currents to the ionosphere obtained in such a manner summed with the fair weather currents is shown in Figure 1 for 18:00 UTC in July under low solar activity conditions. We use different linear color scales for positive and negative current densities since the thunderstorm current density (up to the ionosphere, positive) reaches 180 pA/m^2 above Florida at this time interval while the fair weather currents (down from the ionosphere, negative) have a maximum of about 9 pA/m^2 above the Himalayas. The bold contours separate thunderstorm regions where $J_{atm} > 0$.

In the paper [Blakeslee et al., 2014] the significant role of electrified shower clouds (ESCs, clouds without lightning, which at the same time have a developed electrical structure and contribute to the GEC) is described. Data [Peterson et al., 2018] show that on average ESCs contribute 39% to the total current of GEC while thunderstorms contribute 61%. ESCs would be significant in the frame of our model, but we do not consider them here, since there are no quantitative empirical models of the global distribution of currents into the ionosphere generated by such clouds. The role of electrified shower clouds is also discussed in [Rycroft et al., 2007]. It should also be noted that the accuracy in obtaining the currents for the thunderstorm regions described above is not high. Therefore, despite the high accuracy of the actual calculations as far as the mathematics is concerned, we do not claim a full quantitative description of the GEC. The model should be refined as new empirical models of currents from the troposphere to the ionosphere become available. There is also a very high variability of all the model parameters. For example, we regard all lightning discharges located by WWLLN as being identical. In reality their intensities are different and so they drive different currents up to the ionosphere. That means a redistribution of the currents shown in Figure 1, which cannot be estimated quantitatively. As shown in [Denisenko et al., 2019a], clouds can decrease the total

resistance of the atmosphere by more than a factor of two, and so redistribute atmospheric downward currents to the fair weather regions. That also means a redistribution of the currents shown in Fig. 1; we have to admit that we use rather a simplified model of global cloudiness [Denisenko et al., 2019a].

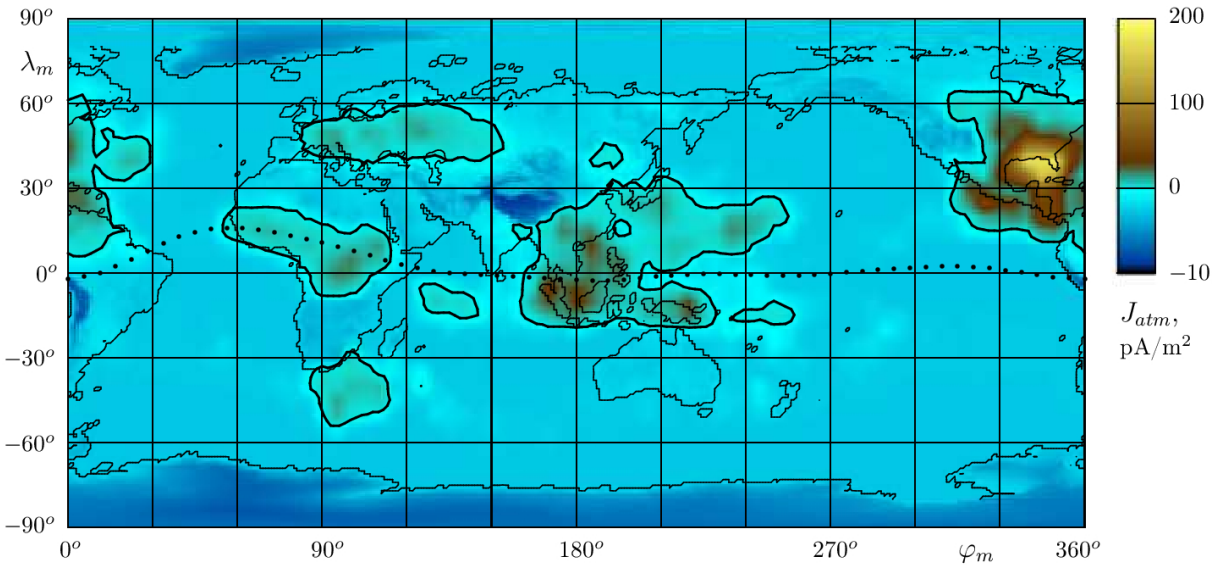

Figure 1. The global distribution of thunderstorm currents to the ionosphere summed with the fair weather currents is shown for 18:00 UT in July 2008 (under low solar activity). Different linear color scales for positive and negative current density J_{atm} are used. The bold contours separate thunderstorm regions where $J_{atm} > 0$. The position of the geomagnetic equator is shown with dots.

4. The 2-D model of the ionospheric conductor

The conductivity of the Earth's ionosphere is a gyrotropic tensor with one axis being defined by the direction of magnetic induction $\boldsymbol{B}$. We use components of the vectors parallel and normal to $\boldsymbol{B}$, which are shown by the symbols $\parallel$ and $\perp$, with $B = \boldsymbol{B}$. Then Ohm's law, Eq. (3), takes the form

$$\boldsymbol{j}_\parallel = \sigma_\parallel \boldsymbol{E}_\parallel, \quad \boldsymbol{j}_\perp = \sigma_P \boldsymbol{E}_\perp - \sigma_H [\boldsymbol{E}_\perp \times \boldsymbol{B}]/B \tag{6}$$

with Hall (σ_H), Pedersen (σ_P) and field-aligned ($\sigma_\parallel$) conductivities [Kelley, 2009]. The conductivities are calculated using the following empirical models:

a) the International Reference Ionosphere, IRI-2016 [Bilitza et al., 2017],
b) the Mass Spectrometer Incoherent Scatter 1990 E [Hedin, 1991], and
c) the International Geomagnetic Reference Field 1945-2010, IGRF [Thébault et al., 2015].

We define the upper boundary of the ionosphere at the height $h_M = 500$ km, above which the typical approximation for the magnetosphere $\sigma_\parallel = \infty$, $\sigma_P = \sigma_H = 0$ is used. The lower boundary of the ionosphere is taken to be at the height $h_I = 80$ km. Below is the atmosphere with isotropic conductivity, that corresponds to the following components of the conductivity tensor: $\sigma_\parallel = \sigma_P$, $\sigma_H = 0$.

When the conductivity in the direction of the magnetic field $\sigma_\parallel$ is a few orders of magnitude larger than σ_P, σ_H it is possible to reduce a three-dimensional model to a two-dimensional one. We use this approximation in the ionosphere between h_I and h_M. Our version of this type of model is presented in [Denisenko et al., 2008].

The electric field $\boldsymbol{E}_\perp$ produces the current $\boldsymbol{j}_\perp$; by Ohm's law, Eq. (6), integrated along a magnetic field line, we obtain the total current across the magnetic field line $\boldsymbol{J}_\perp$ on the left-hand side. If the magnetic field lines were parallel straight lines, then $\boldsymbol{E}_\perp$ would be constant in this integration and so

$$\boldsymbol{J}_\perp = \begin{pmatrix} \Sigma_P & \Sigma_H \\ -\Sigma_H & \Sigma_P \end{pmatrix} \boldsymbol{E}_\perp, \tag{7}$$

with Pedersen and Hall conductances Σ_P, Σ_H (Hargreaves, 1979) which are obtained from the local Pedersen and Hall conductivities σ_P, σ_H by integration along a magnetic field line

$$\Sigma_P = \int \sigma_P \, dl, \quad \Sigma_H = \int \sigma_H \, dl.$$

The signs in Eq. (7) correspond to Eq. (6) in local right hand Cartesian coordinates with the z-axis antiparallel to the magnetic induction vector $\boldsymbol{B}$. Strictly speaking, the magnetic field lines are not parallel straight lines, which introduces some geometric factors in the integration. This is especially important for the summation of Σ_P, Σ_H at conjugate points in the two hemispheres; in the calculations we are careful in this regard.

The empirical model IRI does not present any auroral enhancement of the electron concentration that is produced by high energy electron and proton precipitation from the magnetosphere. The corresponding enhancement of conductivity is usually added as the auroral zones with large conductances Σ_P, Σ_H [Weimer, 1999]. Here we also use the Cowling conductance $\Sigma_C = \Sigma_P + \Sigma_H^2/\Sigma_P$ [Richmond, 1973], which has its greatest importance at low latitudes. The global distribution of Σ_C which is thereby obtained is presented in Figure 2. Dots show the geomagnetic equator, i.e. the position at 120 km height with a horizontal magnetic field. In Figure 2, a logarithmic scale is used since the values vary by about four orders of magnitude. The conductance Σ_C at each half of a magnetic field line is shown in the dot where the line crosses the surface $h = 120$ km; in other words a half of a magnetic field line is substituted with a dot. It must be mentioned that equatorial magnetic field lines, which are below $h = 120$ km, are not shown in this Figure. We would like to stress that this is a problem of visualization only and that it does not exist in the calculations.

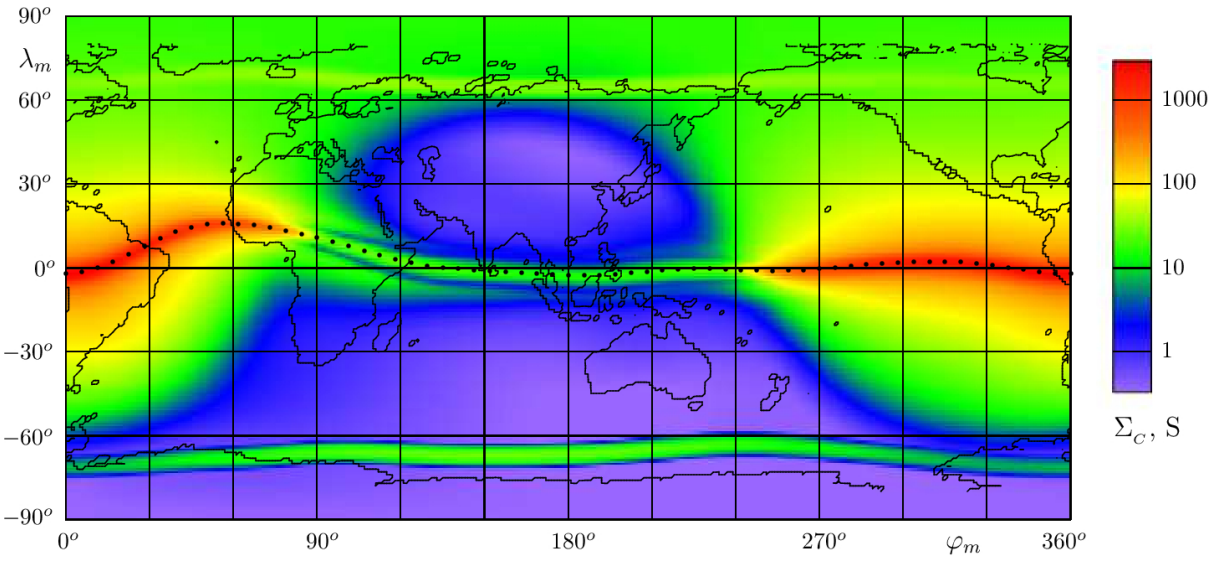

Figure 2. Global distribution of the Cowling conductance Σ_C on a logarithmic scale. The points with λ_m, φ_m geomagnetic coordinates at 120 km height in the ionosphere identify halves of magnetic field lines. The geomagnetic equator is shown with dots. The map is calculated under typical conditions for July 2008 under low solar activity at the considered point in time, 18:00 UT.

We define the geomagnetic equator at the height $h_{eq} = 90$ km as the line $\theta_m = \theta_{eq}(\varphi_m)$, where the magnetic field is horizontal. The function $\theta_{eq}(\varphi_m)$ is found in the frame of the IGRF model. It is natural to identify each magnetic field line with the geomagnetic coordinates θ_m, φ_m of the point at which the line crosses the sphere whose radius corresponds to h_{eq}. It must be done only for the Northern halves of the lines, that means $\theta_m < \theta_{eq}(\varphi_m)$.

The charge conservation law Eq. (5) in the 2-D model is satisfied as integrated along a magnetic field line. It is useful to construct some reference domain at the plane with Cartesian coordinates x, y whose points identify all the magnetic field lines of interest. At such a reference plane, after the necessary geometrical transformation the 2-D current continuity equation can be written as

$$-\frac{\partial}{\partial x}\left(\Sigma_{xx}\,\frac{\partial V}{\partial x}+\Sigma_{xy}\,\frac{\partial V}{\partial y}\right)-\frac{\partial}{\partial y}\left(\Sigma_{yx}\,\frac{\partial V}{\partial x}+\Sigma_{yy}\,\frac{\partial V}{\partial y}\right)=Q, \tag{8}$$

where Q is defined by the atmospheric currents J^N_{atm}, J^S_{atm} entering the ionosphere through the ends of a magnetic field line in the Northern and Southern hemispheres. The details of the necessary transformation of the conductances in Eq. (7) and the right hand side of equation Eq. (5) are given in [Denisenko et al., 2008]. If we consider the dipole approximation of the geomagnetic field the procedure is significantly simplified, and the tensor of the coefficients in Eq. (8) has the same shape as in Eq. (7) [Denisenko and Zamay, 1992].

The right-hand side Q in Eq. (8) as well as J^N_{atm}, J^S_{atm} has two components: those produced by the currents generated by thunderstorms (positive Q since these currents go up in the atmoshere and so deliver positive charges to the ionosphere) and those produced by fair weather currents which deliver charges back to the ground (negative Q). The first component is described in Section 3. The fair weather currents are calculated as the currents in the conducting atmosphere between the ionosphere and the ground because of the given voltage $V_0 = 250$ kV, as described in detail in [Denisenko et al., 2019a]. The value $V_0 = 250$ kV it taken to provide the fair weather vertical electric field strength in air near the ground of $E_0 = 130$ V/m, as discussed in Section 3.

The partial differential equation Eq. (8) of elliptical type with the boundary conditions in the auroral zones and at the geomagnetic equator, which were set in [Denisenko et al., 2019a], has a unique solution [Denisenko, 1994]. Our numerical method for such a problem is described in detail in [Denisenko, 1995, 1998], including a new statement of the boundary value problem, the finite element method, the multigrid method, and some test calculations.

5. The results of the simulations

The solution for the boundary value problem for Eq. (8) in the main part of the ionosphere at 18 UTC is presented in Figure 3. The results obtained using a simplified model of the thunderstorm global distribution have been published recently [Denisenko and Rycroft, 2021]. Here we use the model of the global distribution of thunderstorms obtained from the ground-based WWLLN. It describes real thunderstorm activity better, but also is rather simplified; the situation is discussed in the next Section.

The distribution of the electric potential $V(\varphi_m, \lambda_m)$ at the height $h = 120$ km in the ionosphere is shown by the positions of the equipotentials, which are plotted with a contour interval equal to 5 V. For low values of $|V| < 5$ V, the contour interval is set to 1 V; in Figure 3, these are shown as thin lines, dashed lines meaning negative values.

The maximum potential difference is about 54 V. It is nearly three orders of magnitude smaller than the voltage between the ground and the ionosphere that is 250 kV in the model. The corresponding electric field strength is also small. Its horizontal component does not exceed 20 μV/m. Nevertheless, it is this small electric field which provides the distribution of the ionospheric currents which closes the currents from and to the atmosphere. Recall that, in this paper, only the electric fields created by the tropospheric generators of the GEC are considered. The electric fields at this altitude created by magnetospheric and ionospheric generators are three orders of magnitude larger, especially in the auroral zones.

The position of the maximum value of the ionospheric potential $V = 50$ V corresponds to the large thunderstorm generator over South-Eastern Asia shown in Figure 1. We see only a slight enhancement of the potential above other thunderstorm regions because of the large day-time ionospheric conductivity (near the equator, local midday, at $\varphi_m = 340°$).

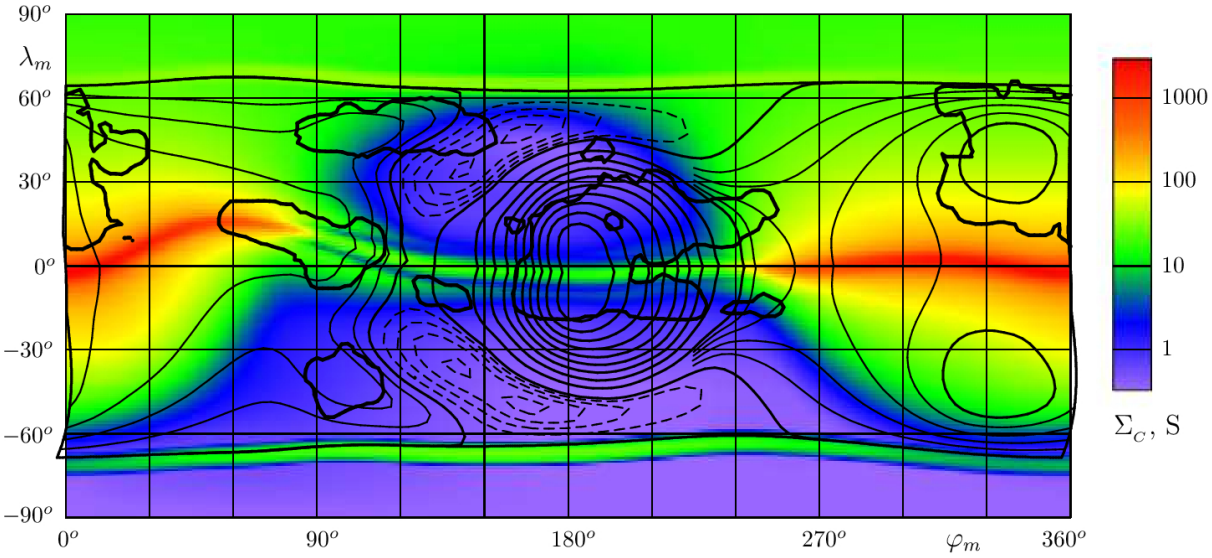

Figure 3. Distribution of the electric potential at 120 km height in the ionosphere. Equipotentials are plotted with a contour interval of 5 V. For low values of $|V| < 5$ V, the contour interval is set to 1 V; these are shown as thin lines. Dashed lines correspond to negative values of potential. The distribution of the Cowling conductance Σ_C is shown by the color scale, as in Fig. 2. The bold contours separate thunderstorm regions where $J_{atm} > 0$, as in Fig. 1. The map is calculated under typical conditions for July under low solar activity at the considered point in time, 18:00 UT.

Minimum values of the potential correspond to fair weather areas, because the electric charges must be delivered there before travelling downwards through the atmosphere as the fair weather currents. This means that there is a negative divergence of the ionospheric electric current Q in equation (8). The minimal values of the negative potential are above the southern part of the Indian Ocean because it is far from thunderstorm regions and because the ionospheric conductivity is small there. It would not be so if the ionospheric conductivity was not also small in the conjugate region that is central Asia. The direction of the electric field is normal to the equipotentials, from large to low values of the potential. In general it corresponds to the direction from the thunderstorms to the fair weather regions.

Figure 3 demonstrates a natural property of the electric field strength: it is much larger in the night-time ionosphere due to the small associated ionospheric conductivity. The distribution of the Cowling conductance Σ_C is shown in Fig. 3 by the color scale, as in Figure 2.

Let us pay attention to the vicinity of the geomagnetic equator where the magnetic field $\boldsymbol{B}$ has a zero vertical component by definition. The geomagnetic equator is shown with dots in Figure 2 and it is clearly seen as the central line of the strip with high conductance in Figure 3. The equipotentials are normal to the geomagnetic equator. Strictly speaking, they are parallel to the magnetic field $\boldsymbol{B}$, and the direction of $\boldsymbol{B}$ is exactly normal to the geomagnetic equator only for a dipolar field. We see variations of the potential along the geomagnetic equator in Fig. 3 which imply a non zero E_φ component of the electric field strength. It is simpler to use the E_x component which is horizontal and normal to $\boldsymbol{B}$, while it does not differ much from E_φ.

Due to the substantial increase of the conductance at the geomagnetic equator, E_x produces the equatorial electrojets [Forbes, 1981]. This field varies slightly with height at the magnetic field lines whose tops are at $H < 200$ km; it does not exceed 20 μV/m. The electrojet current can be obtained by numerical integration as

$$I_{jet}(\varphi_m) = \int_{90\ km}^{135\ km} J_\varphi(\varphi_m, H) dH,$$

where J_φ is defined by Eq. (7) and the chosen height interval corresponds to large values of this component of the current density. The electrojet current is shown by the bold solid line in Figure 4. A positive I_{jet} flows in the eastward direction, and the directions of the electrojets are additionally shown with horizontal arrows. Vertical arrows mark currents up to the ionosphere from the major thunderstorm regions, each arrow corresponding to 100 A at the sector. The other thunderstorm currents are distributed without such a concentration and so are not shown.

One can separate four electrojets in Figure 4, two eastward and two westward, two day-time and two night-time. Midnight is at $\varphi_m = 160°$ and the night-time part of the equatorial ionosphere can be seen as low values of the parameter $A_{jet}(\varphi_m)$ that presents the conductance of the electrojet area as described below. The day-time electrojets are only twice strong as the night-time ones in contrast with electrojets produced by ionospheric and magnetospheric generators for which day/night ratios are as large as two orders of magnitude or more. Often the night-time electrojets can be absolutely ignored because of their small strength. The studied currents from the atmosphere have the same order of magnitude in the day-time and night-time hemispheres. We can say that we are dealing with the atmospheric current generator in contrast with ionospheric and magnetospheric voltage generators.

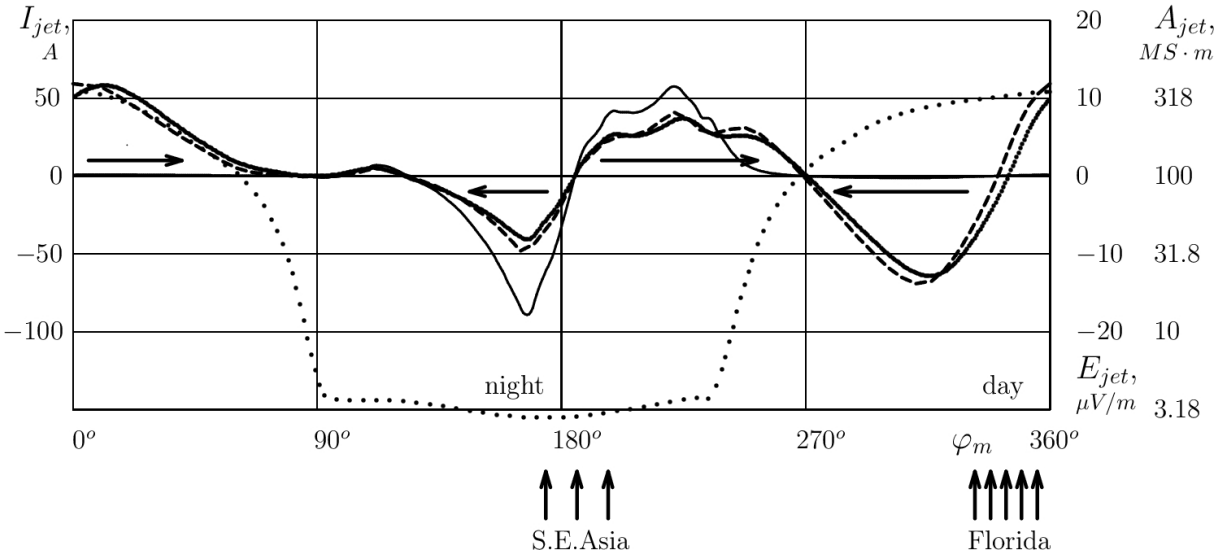

Figure 4. The current of the electrojets $I_{jet}(\varphi_m)$ (bold solid line), the electric field component $E_x(\varphi_m)$ (thin line), the conductance of the electrojet area $A_{jet}(\varphi_m)$ on a logarithmic scale (dotted line) and the product $A_{jet}E_x$ (dashed line). Horizontal arrows show the directions of the electrojets. Vertical arrows mark the currents flowing up to the ionosphere from the major thunderstorm regions; each arrow corresponds to 100 A near that meridian.

An approximate distribution of j_x can be constructed using the theory of the electrojets given by Richmond [1973], in which magnetic field lines are regarded as straight lines in the z direction, the x axis is horizontal, and the y axis is vertical. This theory is based on two simplifications: the component E_x is constant in the plane of a magnetic meridian (y, z) and the vertical current is zero:

$$E_x(x, y) = E_x^0(x),\ J_y = 0$$

Then, from Ohm's law, Eq. (7), we obtain

$$E_y(x, y) = -(\Sigma_H/\Sigma_P)E_x^0(x) \tag{9}$$

$$J_x(x, y) = (\Sigma_P + \Sigma_H^2/\Sigma_P)E_x^0(x),$$

which explains the definition of the Cowling conductance

$$\Sigma_C = \Sigma_P + \Sigma_H^2/\Sigma_P.$$

After integration with respect to y, that is, for all magnetic field lines of the electrojet, we find the total current of the electrojet through this cross-section $x = const$:

$$I(x) = A(x)E_x^0(x) \tag{10}$$

where the conductance of the electrojet area

$$A(x) = \int \Sigma_C(x, y)dy.$$

This parameter, termed $A_{jet}(\varphi_m)$ is shown by the dashed thin line in Figure 4; the product Eq. (10) with $A_{jet}(\varphi_m)$ and $E_x^0(x)$ obtained numerically are also shown. So Figure 4 permits the comparison between the results of our calculations and the simplified theory. The difference $I_{jet} - A_{jet}E_x^0$ is rather small; that favors both approaches, numerical and approximate, since almost the same result is obtained by both calculation procedures. Of course, the approximate theory is not as complete as our full calculations since it needs $E_x^0(x)$ as the input parameter, while it is calculated in the framework of our solution of the boundary value problem for Eq. (8).

The electric field strength $E_x^0(x)$ in this simplified theory has the same direction as the current of the electrojet in accordance with (10), since $A(x) > 0$ as the integral of the positive Cowling conductance. Almost everywhere the directions of I_{jet} and $A_{jet}E_x^0$ coincide. So the horizontal arrows which show the directions of the electrojet current I_{jet} in Fig. 4 also show the directions of the electric field at the geomagnetic equator. These arrows help visualization of the results, while positive I_{jet} and $E_x^0(x)$ already mean eastward directions.

It can be mentioned that the modulus of the electric field strength in the equatorial ionosphere is much larger than its horizontal component, as can be seen in Figures 3 and 4. Above the geomagnetic equator the maximum values of electric field strength are about 620 μV/m and 17 μV/m, respectively. Since the field-aligned component of the electric field equals zero, this means that there is a large vertical component. Because $\Sigma_H \gg \Sigma_P$ in the lower part of an electrojet region, such a large vertical electric field can be explained by the approximate formula Eq. (9).

6. Use of World Wide Lightning Location Network data

Comparison of the electrojets presented in Figure 4 with those calculated for the same conditions in [Denisenko and Rycroft, 2021] (see Figure 9 there) demonstrates a difference. This is due to the significant difference between the simplified model of the global distribution of thunderstorms [Hays and Roble, 1979] used in [Denisenko and Rycroft, 2021] and the model of the global distribution of thunderstorms obtained from the ground-based WWLLN [Denisenko and Lyakhov, 2021] which is used here. Figure 1 shows much weaker currents from the atmosphere up to the ionosphere in Africa and much stronger ones in South-East Asia and in Central America. Because of the redistribution of the generators, all parameters of the electrojets are dramatically varied as also is the electric field global distribution. For example, in the actual model the electric potential attains its maximum above South-East Asia, but not above Africa.

Let us now discuss some features of the data on lightning flashes that has been used. Mezuman et al. [2014] have shown that the WWLLN system observes only 11% of cloud-to-ground discharges, though this value increases up to 30% for those discharges with large currents. This low sensitivity is not a problem in our way of using the data on lightning; it only illustrates that the coefficient of proportionality between the current into the ionosphere and the number of lightning flashes increases. The rather nonuniform lightning detection efficiency over the globe is also a problem with the WWLLN system. As a result of such a nonuniform representation the global distributions of real density of lightnings is distorted and consequently the currents into the ionosphere in our model are perturbed.

Analysis of the satellite data on lightning flash rates in [Mach et al., 2011] shows that the diurnal variation of the total number of flashes does not follow the Carnegie curve. So these authors proposed in [Mach et al., 2010] similar coefficients for lightning discharges of various types, particularly for the ground and ocean. The smaller number of flashes of lightning in the WWLLN data in comparison with satellite data [Blakeslee et al., 2014] should change

those coefficients. Mezuman et al. [2014] and Ccopa et al. [2021] used a transition from the number of lightning flashes to the number of clusters to improve the correlation between WWLLN data and the Carnegie curve. We do not apply such a data processing, because it includes rather arbitrary parameters which lead to remarkably high correlation coefficients, up to 0.99, without taking into account many other factors defining the fair weather electric field. For example, clouds can decrease the total resistance of the atmosphere a few times [Denisenko et al., 2019a] and electrified shower clouds can add up to 40% to the total current [Peterson et al., 2018]. The ability of the "clusterisation" to be used instead of the consideration of the important physical processes means that it contains too many free parameters. Nevertheless, it may be useful after an additional study of its restrictions.

Here we have presented an empirical model of the global distribution of currents into the ionosphere from the atmosphere in which we define the global distribution of this current density as being proportional to the spatial density of thunderstorms. The coefficient is chosen so as to satisfy the Carnegie curve [Harrison, 2013] as described in Section 3. In spite of this simplification, the model used definitely permits us to make an advance on the simple model of [Hays and Roble, 1979].

In future research, we plan to investigate the variation of these ionospheric electrojets with season, Universal Time and solar activity, and including atmospheric currents driven by electrified shower clouds [Rycroft et al., 2007]. Important variations of the GEC and its electrojets are also related to both local and global weather conditions and to thunderstorm activity. Such a set of simulations could permit us to find better conditions for the experimental confirmation of the features of the thunderstorm related part of GEC which are theoretically predicted here. All these influences make the GEC a very complicated object and difficult to deal with, both for measurements and simulations. We shall try to make sequential and significant steps in such simulations. Here we have shown the role of a detailed model of the global distribution of thunderstorms using WWLLN data as one of the available sets of modern data.

7. Conclusions

The electric field associated with the GEC in the ionosphere is mainly defined by the global distribution of thunderstorms delivering charges to the ionosphere and the global distribution of the ionospheric conductance. The importance of a realistic model of the conductance was shown in our previous papers [Denisenko et al., 2019a; Denisenko and Rycroft, 2021] by comparison with the simplified model [Hays and Roble, 1979]. Here we show the role of a detailed model of the global distribution of thunderstorms. Usage of the observed global distribution of thunderstorms obtained from the ground-based WWLLN in [Denisenko and Lyakhov, 2021] has shifted the maximum of the electric potential from Africa to South-East Asia. The equatorial electrojets also change their position, direction and intensity. Nevertheless, they have a similar scale since the total current of the GEC equals 1.43 kA in both models.

The model thunderstorm-related part of the GEC at 18 UTC in July contains four equatorial electrojets, day- and night-time, westward and eastward. Their currents are as large as 65 A. They produce magnetic perturbations on the ground, which are estimated to be in the 0.1 nT range. In principle, these magnetic perturbations could be measured at the night-time geomagnetic equator where they may not be hidden by other electrojets. Our detailed calculations of the electric fields and currents of the electrojets demonstrate good agreement with the 1-D boundary layer model presented by Richmond [1973].

Acknowledgments. This work is supported by the Krasnoyarsk Mathematical Center and financed by the Ministry of Science and Higher Education of the Russian Federation in the framework of the establishment and development of regional Centers for Mathematics Research and Education (Agreement No. 075-02-2022-873).
Our special thanks go to the unknown reviewers for their interest in our line of researches and for their advice for its continuation, as well as for their comments which have permitted us to improve this text.

References

Blakeslee, R. J., D. M. Mach, M. G. Bateman and J. C. Bailey (2014). Seasonal variations in the lightning diurnal cycle and implications for the global electric circuit, Atmos. Res., 135-136, 228-243.

Bilitza, D., D. Altadill, V. Truhlik, V. Shubin, I. Galkin, B. Reinisch and X. Huang (2017). International Reference Ionosphere 2016: From ionospheric climate to real-time weather predictions, Space Weather, 15, 418-429.

Ccopa J.G.A., J. Tacza, J.-P. Raulin and C.A. Morales (2021). Estimation of thunderstorms occurrence from lightning cluster recorded by WWLLN and its comparison with the 'universal' Carnegie curve, J. Atmos. Solar Terr. Phys., 221, 105682.

Denisenko, V. V. (1994). A boundary value problem for an elliptic equation in two variables with asymmetric tensor coefficients, Siberian Math. J., 35, 3, 495-505.

Denisenko, V. V. (1995). Energy methods for elliptic equations with asymmetric coefficients (in Russian), Publ. house Russ. Acad. Sci. Siberian Branch, Novosibirsk.

Denisenko, V. V. (1998). Multigrid method for a global Hall conductor in the Earth's ionosphere, in Virtual Proceedings of the 10-th Anniversary International GAMM - Workshop on Multigrid Methods. http://www.mgnet.org/mgnet-parmgm98.html.

Denisenko, V. V. (2018). 2-D model of the global ionospheric conductor connected with the magnetospheric conductors, Cornell University Library. http://arxiv.org/abs/1802.07955.

Denisenko, V.V., H. K. Biernat, A. V. Mezentsev, V. A. Shaidurov and S. S. Zamay (2008). Modification of conductivity due to acceleration of the ionospheric medium, Ann. Geophys., 26, 2111-2130.

Denisenko, V. V. and A. N. Lyakhov (2021). Comparison of ground-based and satellite data on spatiotemporal distribution of lightning discharges under solar minimum, Solar-Terr. Phys., 7, 4, 104-112.

Denisenko, V. V. and M. J. Rycroft (2021). The Equatorial Electrojets in the Global Electric Circuit, J. Atmos. Terr. Phys., 221, 3, 105704.

Denisenko, V.V., M. J. Rycroft and R. G. Harrison (2019a). Mathematical Simulation of the Ionospheric Electric Field as a Part of the Global Electric Circuit, Surv. Geophys., 40, 1, 1-35.

Denisenko, V. V., M. J. Rycroft and R. G. Harrison (2019b). Correction to: Mathematical Simulation of the Ionospheric Electric Field as a Part of the Global Electric Circuit, Surv. Geophys., 40, 1, 37.

Denisenko, V.V. and O. E. Yakubailik (2015). The income of topography to the resistance of the global atmospheric conductor (in Russian), Solar-Terr. Phys., 1(1), 104-108.

Denisenko, V. V. and S. S. Zamay (1992) Electric field in the equatorial ionosphere, Planet. Space. Sci., 40, 7, 941-952.

Forbes, J. M. (1981). The Equatorial Electrojet, Rev. Geophys., 19, 469-504.

Fujita S., T. Kikuchi and T. Tanaka. (2010). State transition of the magnetosphere-ionosphere compound system due to a northward turn of the interplanetary magnetic field revealed from a global magnetohydrodynamic simulation and formation of the overshielding potential, J. Geophys. Res.: Atmosph., 115, A11210.

Hays, P. B. and R. G. Roble (1979). A quasi-static model of global atmospheric electricity. 1. The lower atmosphere, J. Geophys. Res., 84, A7, 3291-3305.

Hargreaves, J. K. (1979) The upper atmosphere and solar-terrestrial relations. Van Nostrand Reinhold Co Ltd, New York.

Harrison, R. G. (2013). The Carnegie Curve, Surv. Geophys., 34, 209-232.

Hedin, A. E. (1991). Extension of the MSIS Thermospheric Model into the Middle and Lower Atmosphere, J. Geophys. Res., 96, 1159-1165.

Hutchins, M. L., R. H. Holzworth and J. B. Brundell (2014). Diurnal variation of the global electric circuit from clustered thunderstorms, J. Geophys. Res. Space Physics, 119, A019593.

Kelley, M. C. (2009). The Earth's ionosphere: plasma physics and electrodynamics, Academic Press, Burlington.

Klimenko, M. V. and V. V. Klimenko (2012). Disturbance dynamo, prompt penetration electric field and overshielding in the Earth's ionosphere during geomagnetic storm, J. Atmos. Solar Terr. Phys., 90-91, 146-155.

Kudintseva, I. G., A. P. Nickolaenko, M. J. Rycroft and A. Odzimek (2016). AC and DC global electric circuit properties and the height profile of atmospheric conductivity, Ann. Geophys., 59, 5: A0545.

Lunxiang, P., L. Dongxia, Q. Xiushu, et al. (2013) Land-sea contrast in the lightning diurnal variation as observed by the WWLLN and LIS/OTD data. Acta Meteor. Sinica, 27, 4, 591-600.

Mach, D. M., R. J. Blakeslee and M. G. Bateman (2011). Global electric circuit implications of combined aircraft storm electric current measurements and satellite-based diurnal lightning statistics, J. Geophys. Res., 116, D05201.

Mach, D. M., R. J. Blakeslee, M. G. Bateman and J. C. Bailey (2010). Comparisons of total currents based on storm location, polarity, and flash rates derived from high-altitude aircraft overflights, J. Geophys. Res., 115, D03201.

Mezuman K., C. Price and E. Galanti (2014). On the spatial and temporal distribution of global thunderstorm cells, Environ. Res. Lett., 9, 12, 124023.

Minobe, S., J. H. Park and K. S. Virts (2020). Diurnal Cycles of Precipitation and Lightning in the Tropics Observed by TRMM3G68, GSMaP, LIS, and WWLLN. J. Climat, 33, 4293-4313.

Peterson, M., W. Deierling, C. Liu, D. Mach and C. Kalb (2018). A TRMM assessment of the composition of the generator current that supplies the Global Electric Circuit, J. Geophys. Res.: Atmosph., 123, 8208-8220.

Peterson, M., D. Mach and D. Buechler (2021). A global LIS/OTD climatology of lightning Flash Extent Density. J. Geophys. Res.: Atmospheres, 126, e2020JD033885.

Richmond, A. D. (1973). Equatorial electrojet. 1. Development of a model including winds and instabilities, J. Atmos. Terr. Phys., 3, 6, 1083-1103.

Richmond, A. and A. Maute (2014). Ionospheric electrodynamics modeling, Modeling the Ionosphere-Thermosphere System. 57-71.

Rodger, C. J., J. B. Brundell, R. L. Dowden and N. R. Thomson (2004). Location accuracy of long distance VLF lightning location network. Ann. Geophys, 22, 747-758.

Rudlosky, S. D. and D. T. Shea (2013). Evaluating WWLLN Performance Relative to TRMM/LIS, Geophys. Res. Lett., 40, 1-5.

Rycroft, M. J., S. Israelsson and C. Price (2000). The global atmospheric electric circuit, solar activity and climate change, J. Atmos. Sol.-Terr. Phys., 62, 17, 1563-1576.

Rycroft, M., A. Odzimek, N. Arnold, M. Füllekrug, A. Kułak and T. Neubert (2007). New model simulations of the global atmospheric electric circuit driven by thunderstorms and electrified shower clouds: The roles of lightning and sprites. J. Atmos. Sol.-Terr. Phys, 69, 17-18, 2485-2509.

Thébault, E., C. C. Finlay, C. D. Beggan, et al. (2015). International Geomagnetic Reference Field: the 12th generation, Earth Planet Space, 67, 79.

Weimer, D. R. (1999). Substorm influence on the ionospheric electric potentials andcurrents, J. Geophys. Res., 104, 1, 185-197.

***CORRESPONDING AUTHOR: Michael J. RYCROFT**,
CAESAR Consultancy, 35 Millington Road,Cambridge CB3 9HW, UK
e-mail: michaelrycroft@btinternet.com